COMPARATIVE STUDY OF SLAG RESISTANCE OF Al_2O_3-MgO CASTABLES CONTAINING DIFFERENT LIGHTWEIGHT CORUNDUM AGGREGATES

Yang Zou, Huazhi Gu, Ao Huang, Meijie Zhang, Mintao Zhang

State Key Laboratory of Refractories and Metallurgy, Wuhan University of Science and Technology, China

ABSTRCT

Corundum-spinel castables containing lightweight aggregate has drawn many attentions due to its potential for energy-saving, especially when applied in high-temperature region, such as the work lining of refining ladle. One main aspect that restricts its application is the slag corrosion performance. In this study, one dense tabular corundum and three lightweight corundum were chosen as aggregates to prepare four different corundum-spinel castables. The slag resistance was compared through induction furnace corrosion test. SEM-EDS, XRD, and thermodynamic and kinetics analysis were adopted for the discussion of corrosion mechanism. Results showed that the crystal grain size and shape of aggregates were importance for the slag corrosion resistance of lightweight corundum-spinel castables under dynamic condition (enforced convection), yet the effects of pore characteristics were not dominating. Aggregates with large flake-like crystal grain showed thicker dissolution diffusion boundary layer and lower dissolution rate, resulting a favorable corrosion resistance of the castable. Poor microstructure of the aggregates -- larger pores and small and spherical grains, would cause deterioration of castables' slag resistance performance.

KEYWORDS

1 INTRODUCTION

Development of new high-refractory materials for thermal insulation is a very important task since these refractories can improve the technical and economic performance of the furnaces and thermal units in high-temperature industry. To this end, extensive studies on lightweight aggregate and corresponding lightweight wear lining refractories have been carried out [1–3]. Although favorable heat-shielding and thermal shock resistance performance of lightweight refractories have been shown in many of these studies, the application of lightweight refractory is still restricted from serving as work-lining material (eg. the hot-face of a ladle) due to an inferior slag corrosion resistance.

As to the slag corrosion mechanism of alumina/ magnesia/spinel refractories, many studies have been done [4, 5]. Most pointed out that the formation of continuous solid phases layer (eg. $CaAl_{12}O_{19}$) can result in indirect dissolution of refractories [6, 7] and prevent the alumina and spinel from a lime-rich slag corrosion [8]. In spite of these valuable results, the refractories in above studies were actually under static condition, which was not necessary the same as that of real refining process. Since slag was always in motion in practice, of which the effects on refractories' slag resistance cannot be neglected, some researchers also adopted dynamic method to investigate the slag corrosion of certain refractory. Kim Fagerlund [9] measured the dissolution rate of silica rods in an iron-saturated silicate slag containing 15–30% SiO_2 using the rotating cylinder technique, and found that the Marangoni effect was significant under stagnant conditions, but gradually became dominated by bulk flow when the linear velocity of flowing melt was increased. Li[10] investigated the influence mechanism of electromagnetic field (EMF) speeding up the corrosion of low carbon MgO–C refractories using an induction furnace, their result showed that EMF restrained the formation of MgO dense layer, and induced a more severe corrosion of the material.

However, with regard to the slag corrosion of lightweight Al_2O_3-MgO castable under dynamic corrosion condition, few researches has been reported. In this paper, discussion was focused on the effects of aggregates' microstructure on slag resistance of lightweight corundum-spinel castable. The corrosion performance of three lightweight castables, of which the lightweight corundum aggregates had different microstructure, was investigated through induction furnace corrosion test, and the results were compared with that of a common corundum-spinel castable containing tabular corundum aggregates. XRD, SEM-EDS, and thermodynamic calculation were adopted for the discussion of corrosion mechanism.

2 EXPERIMENT

2.1 Raw Material and Sample Preparation

One dense tabular corundum (denoted as TC) and three lightweight corundum (denoted as L1, L2 and L3) were chosen as aggregates to prepare four different corundum-spinel castables (denoted as CTC, CL1, CL2, and CL3 respectively). The pore characteristic parameters of the four aggregates including apparent porosity (AP), closed porosity (CP), average pore size ($D_{m\_4V/A}$) and the median pore diameter (D_{50}) were given in Tab.1.

Tab.1: Pore characteristics of different corundum aggregate

Aggregates	Apparent porosity (%)	Closed porosity (%)	D_{50} (μm)	$D_{m\_4V/A}$ (μm)
TC	4.93	3.3	0.75	0.34
L1	4.52	7.8	0.49	0.45
L2	10.9	4.5	0.58	0.48
L3	19.4	0.7	2.8	2.6

Matrix was composed of white corundum powder (Jiangsu Jingxin High-Temperature Materials Co., Ltd., Jiangsu, China), reactive α-Al_2O_3 micro-powder (Kaifeng Special Refractory Co., Ltd., Henan, China), Secar 71 cement (LAFARGE ALUMINATES, Al_2O_3 > 68.5wt%, CaO > 31.0wt%, D_{95} < 90μm), fused magnesia powder (MgO > 97.2 wt%, D_{50} =22.64μm), and MgO micro-powder. After weighing, the raw materials were mixed with 0.15 wt% FS10 dispersant (BASF Construction Polymers GmbH, Trostberg, Germany) and 4.5 wt% water in a mixer and then were casted into 25 × 25 × 125 mm^3 samples by vibration. After curing at room temperature for 24 h, samples were dried at 110 ℃ for 24 h.

The composition of the pre-melted slag for corrosion test was shown in Tab.2. They were prepared by melting regent-grade CaO, SiO_2, and Al_2O_3 in a graphite crucible at 1773K in a muffle furnace with reduction atmosphere.

Tab.2: Chemical composition of slag after pre-melting (wt %)

Composition	Al_2O_3	CaO	SiO_2
amount	24	41.4	34.6

2.2 Tests and Examination Methods

The samples after drying were casted into the lining of an

intermediate frequency induction furnace. 2.7 kg steel were filled into the furnace and heated under an alternative electromagnetic field with a frequency ~ 3500 Hz. 70.0 g of slag was added into the furnace after melting of steel. The temperature was kept in the range 1600~1625℃ for 40mins to carry out the slag resistance experiments under dynamic condition. By reaching the pre-supposed time, the steel and remain slag were poured out immediately, then a natural cooling was followed.

The pore-size distribution and average pore-diameter of different aggregates were measured by mercury intrusion porosimetry measurement (AutoPore IV 9500, Micromeritics Instrument Corporation). Apparent corrosion depth of the samples were measured using program Image-Pro plus 6.0 (Media Cybernetics, America). Phases of corroded sample were analyzed by X-ray diffractometer (XRD, X'Pert pro). Microstructure analysis were carried out using scanning electron microscope (SEM, JSM-6610, JEOL, Tokyo, Japan) and energy dispersive spectrometer (EDX; QUANTAX, Bruker, Berlin, Germany). Thermodynamic calculation was performed with commercial software FactSage v 6.4.

3 RESULTS AND DISCUSSION

3.1 Apparent Corrosion Depth

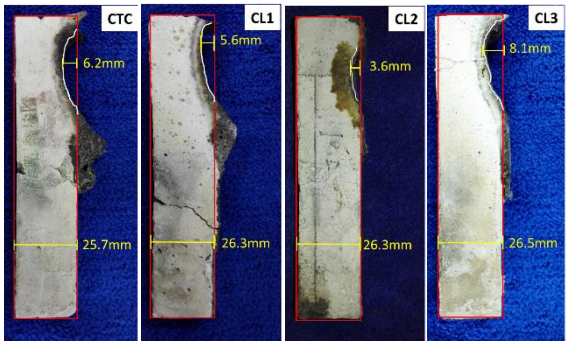

Fig.1: Apparent appearance of different Al_2O_3-MgO castable CTC, CL1, CL2, and CL3 after corrosion test

The apparent appearance of four Al_2O_3-MgO castable after corrosion test were shown in Fig.1, in which the corrosion depth of each sample was marked. As shown in the figure, the Al_2O_3-MgO castables contain tabular corundum TC and lightweight corundum L1 as aggregates had similar slag resistance, of which the apparent corrosion depth were 6.2mm and 5.6mm respectively. The slag resistance of sample containing aggregate L2 was the best, by giving an apparent corrosion depth of 3.6mm. Sample with L3 as aggregates showed the worst slag resistance (apparent corrosion depth 8.1mm). .

3.2 Microstructure

3.2.1 Interface of slag and aggregates

Since the only differences among the four castables are aggregates, the microstructure of the four corundum need to be compared carefully.

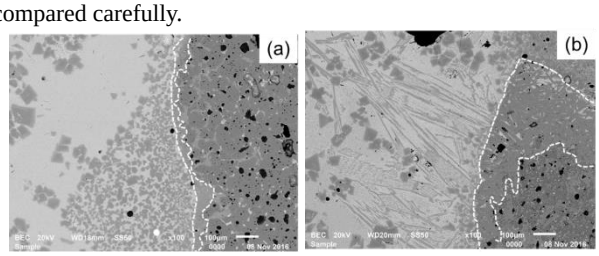

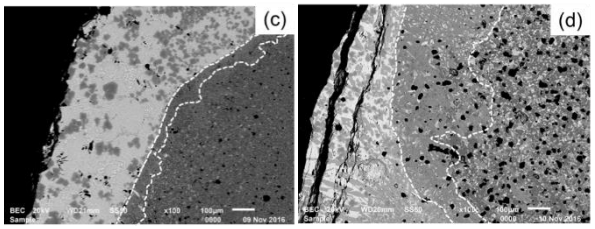

Fig.2: micro-features of the aggregates of four castables after slag corrosion, (a) TC; (b) L1; (c) L2; (d) L3

The microstructure of aggregates after corrosion were shown in Fig.2. As shown in the figure, the corroded area of L1 and L3 after 40mins test were significantly larger than that of TC and L2. It can also be seen that interior part of lightweight corundum L3 has been penetrated by slag. As this only happen for L3, it is suggested that the slag resistance of L3 was the worst.

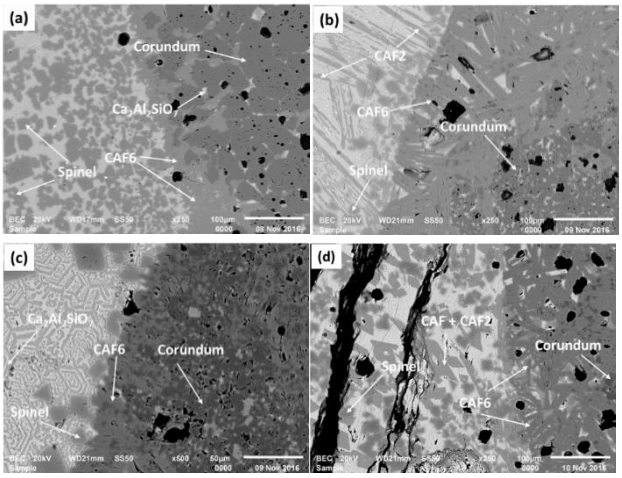

Fig.3: Phase distribution of four different aggregates after slag corrosion, (a) TC; (b) L1; (c) L2; (d) L3

The mineral phase distribution of four aggregates TC, L1, L2, and L3 after a 40mins reaction with slag were given in Fig.4. The main phases located in the corroded area for all the four corundum aggregates was corundum (Al_2O_3), CA_6 and Spinel. Besides that, CAF_2 was also detected in the slag-aggregates interface zone for L1 and L3. For L2, there were a large amount of $Ca_2Al_2SiO_7$ existing at the slag-aggregates interface, and this phase only barely detected in the corrosion interface of TC.

3.2.2 Microstructure characteristics of different corundum

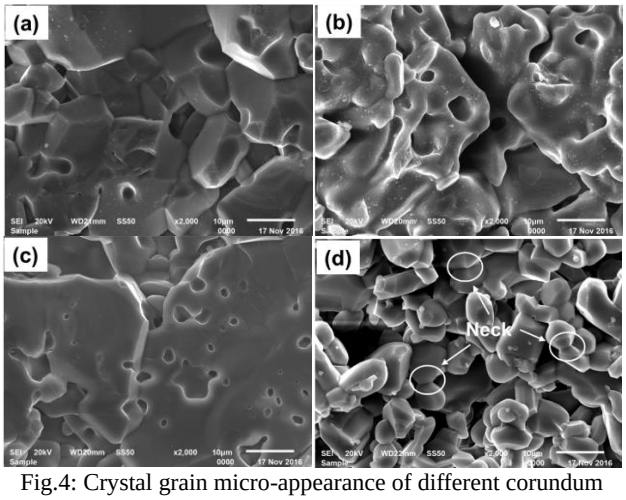

Fig.4: Crystal grain micro-appearance of different corundum aggregates, (a) TC; (b) L1; (c) L2; (d) L3

The fracture micro-appearance of four corundum aggregates TC, L1, L2 and L3 were given in Fig.4. It can been seen that the

crystal grain size of aggregate L3 was significantly smaller than that of the other three aggregates. Besides crystal grain size, the crystal grain shape and contact state are also different. The crystal grain shape of TC was polyhedral, and most of the crystal grain showed equal-axial characteristics. In contrast to this, the internal grain of L2 had the structure of layered stack, and grain size in length and width direction were more than 60um, but the thickness was less than 5um. Aggregates L1 contain irregularly-shaped crystal grains, which contacted to each other loosely. The internal crystal grain of L3 had spherical shape, of which the neighboring crystal grains contacted to each other by point. The existence of 'neck' indicated an inadequate sintering of L3.

3.3 XRD Analysis

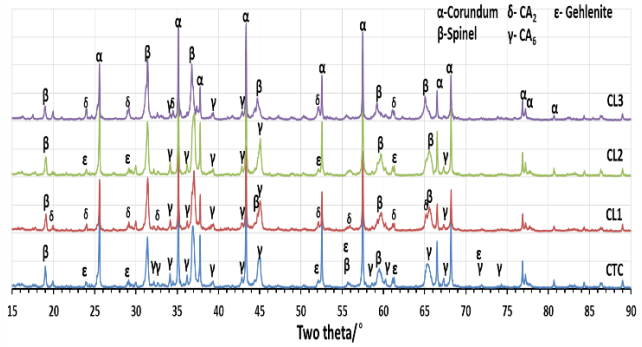

Fig.5: XRD patterns of sample containing different corundum aggregates after corrosion test

The XRD pattern of four Al_2O_3-MgO castables after corrosion test were given in Fig. 5. The samples for XRD analysis were prepared by cutting the material located in slag/castables interface with a thickness 2mm, and then grinding it in an agate mortar. It can been seen that all the mineral phases determined in XRD analysis was consistence with the results of EDS detection, of which corundum, spinel, and CA_6 were detected in all samples. Gehlenite ($Ca_2Al_2SiO_7$) was only found in the sample CTC and CL2, while a small quantities of CA_2 were detected in sample CL1 and CL2

Since the intensity of the strongest peak corresponding to certain phase in XRD diffraction pattern can reflect the relatively amount of that phase in a mixture, a semi-quantified analysis was carried out by calculating the ratio of the peak intensity of spinel and CA_6 relative to corundum, and the results were given in Tab.3.

Tab.3: Semi-quantified amount of phases located at castable-slag interface

	relative intensity of main peaks				
	Al_2O_3	$MgAl_2O_4$	CA_6	CA_2	C_2AS
CTC	100	42.6	7.4	-	20.3
CL1	100	70.3	9.6	uc	-
CL2	100	45.7	7.2	-	22.9
CL3	100	56.3	8.2	uc	-

'-'..no corresponding phase detected
'uc'.. Cannot determine relative intensity due to peak overlapping

As shown in the Table, the CA_6 content identified in sample CL1 and CL3 was significantly higher than that of CTC or CL2, of which CL2 has the least CA_6 content identified at the slag-castable interface. Since CA_6 was the main product of the reaction between corundum and a lime-rich slag [5], and the matrix of all four sample were identical, the amount of CA_6 detected at slag-castable interface can qualitatively reflect the severity of slag corrosion of corundum aggregates. It can be deduced from Tab.2 that the slag resistance of CTC, CL1, CL2 and CL3 in this study are CL2>CL1≈CTC>CL3.

3.4 Thermodynamic and Kinetic Analysis

In this study, thermodynamic calculation was carried out by adopting the commercial program FactSage. The "Eqiuilib" module was chosen, and databases "FactPS" and "FToxide" was used. Since composition non-uniform and local dissolution during corrosion were possible to take place, three situations including the dissolution of matrix or aggregates independently, and the simultaneously dissolution of aggregate and matrix were considered. A parameter "Alpha" was used to represent the amount of refractory component dissolved in the slag, which was defined as:

$$\text{Alpha} = \frac{mass_{mater}}{100} \quad (1)$$

Where $mass_{mater}$ was the castable component (matrix or aggregates or both) dissolved in the slag. The results were given in Fig.6.

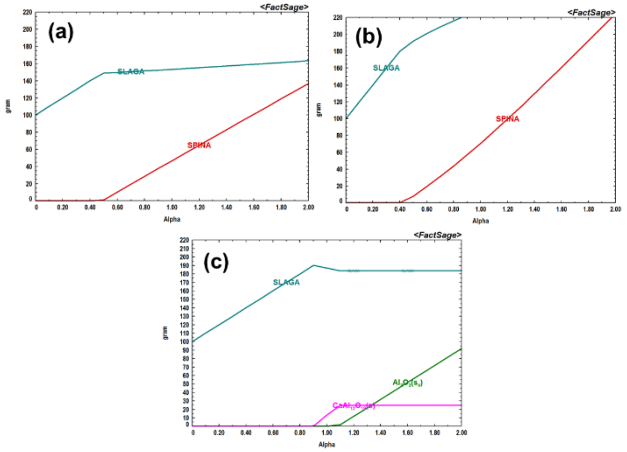

Fig.6 Phases evolution with a continuous dissolution of castables component into slag, (a) matrix; (b) matrix and aggregates; (c) aggregates

Fig.6 shows the evolution of phase amount at the slag-material interface with a continuous dissolution of castables component. As it shows, spinel generated with the condition of the independently dissolution of matrix or the simultaneously dissolution of matrix and aggregates. For the latter, spinel was generated more and faster (the curve corresponding to spinel in Fig.7-(b) has larger slope than that of Fig.7-(a)). From Fig.7-(c) it is suggested that CA_6 only exist when aggregates dissolve solely. Since CA_6 was detected in all the four samples (section 3.2.1), it can be deduced that the composition non-uniform and local dissolution of aggregates happened during the corrosion process.

Combining the analysis above with the SEM-EDS detection results in section 3.2, it can be concluded that the different dissolution speed of corundum aggregates caused the distinct amount and distribution of CA_6 and $Ca_2Al_2SiO_7$ in the slag-aggregates interface of four castables. The corrosion of Al_2O_3-MgO castables by the Al_2O_3-CaO-SiO_2 slag introduced CA_6 being generated at the outer layer of corundum aggregates, along which the spinel in castable matrix dissolved at first and then re-precipitated from the saturated slag (liquid).

A lot of study [4, 9, 10] point out that the dissolution of refractory in slag was dissolution controlled. The dissolution rate can be determined based on the Fick's law.

$$\frac{Dc}{Dt} = \frac{D_{eff}}{\delta} \cdot (C_s - C_m) \cdot \mathrm{A} \quad (2)$$

In above equation, D_{eff} is the diffusion coefficient, m^2/s; Cs donates the saturated concentration of castable component in slag, g/cm^3; C_m is the initial concentration of castable component, g/cm^3; δ is the thickness of diffusion boundary layer, m; A donates

the contact area between slag and castable, m^2.

According to the kinetics similarity of a plate dissolved in liquid under enforced convection, the diffusion boundary layer thickness of a corundum crystal grain dissolved in the slag follow the empirical formula as,

$$\delta = 3.09(\frac{x}{U})^{\frac{1}{2}} \cdot D_{eff}^{\frac{1}{3}} \cdot v^{\frac{1}{6}} \quad (3)$$

Where x is characteristics length, which is defined by the distance from dissolution region to slag/material interface, m; U is enforced flow velocity, m s^{-1}; v is the kinematic viscosity, m^2/s.

Following flux equation can be obtained:

$$\frac{Dc}{Dt} = \frac{D_{eff}^{\frac{2}{3}}}{3.09} \cdot (c_s - c_m) \cdot A \cdot (\frac{U}{x})^{\frac{1}{2}} \cdot v^{-\frac{1}{6}} \quad (4)$$

In the study, since the experiment condition was virtually identical, the parameters D_{eff}, C_s, C_m, v and U were also the same for all four sample. It is A $x^{-0.5}$ that resulted in the different slag resistance of four Al_2O_3-MgO castable. As it is difficult to determine the value of $x^{0.5}/A$, the microstructure features of the four different corundum including shape and size of the aggregates crystal grain, and resultant A, x and finally $x^{0.5}/A$ were summarized to compared the effects of microstructure of corundum aggregates on dissolution qualitatively, as shown in Tab.3.

Tab.3: Qualitatively compare of $x^{0.5}/A$ of four corundum aggregate

	grain shape	grain size(μm)	A (m^2)	X (m)	$x^{0.5}/A$
TC	Polyhedron	20-40	small	medium	medium
L1	Irregular	30-40	medium	medium	medium
L2	flake-like	50-80	small	large	large
L3	spherical	5-15	large	small	small

According to the Table, for four different corundum aggregates TC, L1, L2 and L3, the dissolution flux with a large to small sequence should be: L3>L1>TC>L2. According the analysis in section 3.4.1, the dissolution of corundum was companied by the generation of CA_6 and re-precipitation of spinel at slag/castables interface. The amount of CA_6 and spinel located at slag/castables interface of four castable should also be: L3>L1>TC>L2. Recalling the semi-quantitative results of the CA_6 and spinel content in Tab.3, the kinetics analysis above are almost in full accordance with the slag corrosion experiment.

CONCLUSIONS

One dense tabular corundum and three lightweight corundum were chosen as aggregates to prepare four different corundum-spinel castables, and the slag resistance of these refractories was compared. Results showed that the crystal grain size and shape of aggregates were important for the slag corrosion (dissolution) resistance of lightweight corundum-spinel castables under enforced convection, yet the effects of pore characteristics were not dominating. For CL2, the favorable corrosion resistance was mainly due to the large size and flake-like shape of aggregate crystal grain, resulting a thicker diffusion boundary layer and lower dissolution rate. CL1 and CTC showed similar acceptable corrosion performance, of which the former was contributed to the small and even pore distribution of aggregates L1, but the latter was mainly a result of aggregates' grain features. The inferior microstructures (larger pores and small spherical crystal grains) of aggregates caused the deterioration of slag resistance of castable CL3.

ACKNOWLEDGEMENTS

This work was financially supported by the National Natural Science Foundation of China (Grant nos. 51204126 and 51474165).

REFERENCES

[1] Yan W, Li N, Han B Q. Effects of microsilica content on microstructure and strength of lightweight castable refractories containing porous corundum-spinel aggregate. Science of Sintering, 2009, 41(3):275-281.

[2] Chen X, Penumadu D. Characterizing microstructure of refractory porous materials. Journal of Materials Science, 2006, 41(11):3403-3415.

[3] Kaneko T K, Zhu J, Thomas H, et al. Influence of Oxygen Partial Pressure on Synthetic Coal Slag Infiltration into Porous Al $_2O_3$, Refractory. Journal of the American Ceramic Society, 2012, 95(5):1764–1773.

[4] Lee W E, Zhang S. Melt corrosion of oxide and oxide–carbon refractories. International Materials Reviews, 1999, 44(3):77-104.

[5] Braulio M A L, Martinez A G T, Luz A P, et al. Basic slag attack of spinel-containing refractory castables. Ceramics International, 2011, 37(6):1935-1945.

[6]Martinez A G T, Luz A P, Braulio M A L, et al. CA 6, impact on the corrosion behavior of cement-bonded spinel-containing refractory castables: An analysis based on thermodynamic simulations. Ceramics International, 2014, 41(3):4714-4725.

[7] Sako E Y, Braulio M A L, Pandolfelli V C. The corrosion and microstructure relationship for cement-bonded spinel refractory castables. Ceramics International, 2012, 38(3):2177-2185.

[8] Fu L, Gu H, Huang A, et al. Slag Resistance Mechanism of Lightweight Microporous Corundum Aggregate. Journal of the American Ceramic Society, 2015, 98(5):1658-1663.

[9] Fagerlund K, Sun S, Jahanshahi S. Effect of Marangoni-induced flow on the rate of refractory dissolution in molten slags. Scandinavian Journal of Metallurgy, 2002, 31(6):359–366.

[10] Li X, Zhu B, Wang T. Electromagnetic field effects on the formation of MgO dense layer in low carbon MgO, C refractories. Ceramics International, 2012, 38(4):2883-2887.